# Blind Deconvolution Methods for Estimation of Multilayer Tissue Profiles with Ultrawideband Radar

Burak Cevat Civek, Nithin Sugavanam, Siddharth Baskar, Emre Ertin
Department of Electrical and Computer Engineering
The Ohio State University, Columbus
civek.1@osu.edu

Abstract—Sensors that can rapidly assess physiology in the clinic and home environment are poised to revolutionize research and practice in the management of chronic diseases such as heart failure. Ultrawideband (UWB) radar sensors provide a viable and unobtrusive alternative to traditional sensor modalities for physiological sensing. In this paper, we consider the problem of estimation of multilayer tissue profiles using an ultrawideband radar sensor. We pose the joint estimation of the ultrawideband pulse waveform and the multilayer tissue profile as a blind deconvolution problem. We show that constraints on the pulse waveform (bandwidth and time duration) and the structure of tissue range profile (sparsity) can be used to regularize the inversion. We derive both convex and non-convex algorithms for the joint estimation of the pulse waveform and the tissue reflectivity profile and demonstrate the effectiveness of the proposed methods with measured and simulated data experiments.

### I. Introduction

Sensors that can rapidly assess physiology in the clinic and home environment are poised to revolutionize research and practice in diagnosing and treating health conditions and long-term chronic disease care [1]. RF frequencies penetrate all skin, fat, muscle tissue and therefore provide a viable alternative to traditional modalities of ECG and Ultrasound for sensing of physiology without requiring electrodes, conductive gels or cuffs. In particular, if an ultrawideband (UWB) radar sensor is used to interrogate human body, each tissue interface (air-skin, skin-muscle, muscle-bone, etc.) causes a different reflection point to the impinging wideband pulses providing a rich backscatter signal [2], [3], [4], [5] that can inform on tissue composition and motion.

Specifically, ultrawideband radar sensing provides a unique opportunity to monitor pulmonary and peripheral edema-water retention in home and clinic environments. Technological advances in earlier detection of edema have revolved around measurements of transthoracic and intrathoracic impedance using implanted sensors. As electromagnetic (EM) wave propagation in the body is affected strongly by the dielectric properties of the tissues, radar-based sensors show promise as a non-invasive tool to monitor fluid retention in the lungs that can replicate the utility of these implanted diagnostic systems without requiring expensive procedures.

However, near-field on-body measurements with a UWB radar sensor raises significant technical challenges. The transmitted UWB waveform from the antenna is highly dependent on the antenna-skin interface and can have high inter-subject

variability. Even for the same subject antenna transfer function can change based on the placement and skin conditions. As a result, tissue properties have to be estimated from radar returns jointly with the transmitted waveform. In addition, high-resolution recovery is required to resolve multiple layers of tissue in range, which can be only accomplished by incorporating prior information on the unknown reflectivity profile.

In the following, we pose the blind deconvolution problem of jointly estimating the pulse waveform and the multi-layer tissue profile and provide both convex and non-convex methods for its solution, exploiting known structure in the transmitted waveform and the reflectivity profile of the tissues. We illustrate the effectiveness of the proposed methods using experiments with measured and simulated data.

## II. SYSTEM MODEL

We consider a monostatic ultrawideband radar sensor that transmits a short duration UWB pulse,  $\boldsymbol{h} \in \mathbb{R}^T$ , and records the backscattered signal from a near field object composed of multiple layers of dielectric material. Let the vector  $\boldsymbol{y} \in \mathbb{R}^N$  denote N time samples of the received backscatter signal, which is modeled as the linear convolution of the reflectivity profile of the multilayer dielectric media  $\boldsymbol{x} \in \mathbb{R}^{N-T+1}$ , with the unknown pulse waveform  $\boldsymbol{h}$ 

$$y = h * x. (1)$$

While the electric pulse feeding the antenna can be characterized precisely, in a setting where the antenna is placed on the body directly, there is considerable uncertainty in the transmitted waveform because the wideband antenna characteristics are highly variable with respect to the antenna-skin interface. Therefore, we formulate the problem as blind deconvolution, where we aim to recover both the transmitted pulse h and the tissue profile x jointly using the measurement y. The blind deconvolution problem is a highly ill-posed bilinear problem and inherently suffers from identifiability problems due to the scale and shift ambiguities between h and x. The reasons for non-identifiability are due to an orthonormal transformation ambiguity [6], [7], [8] (which generalizes the shift and rotational ambiguity), scaling ambiguity and a trivial global optima [9] such that the solution is  $\hat{h} = y$  the measurement and  $\hat{x} = \delta$  the Kronecker delta function for the class of loss functions and regularizing functions that are

commonly used in blind deconvolution. Recent works [10], [11] have established requirements on the structure of the signals and the number of measurements required to make the problem identifiable. Non-convex algorithms exploiting the structure in the signals were also proposed. However, these methods rely on the unstructured basis functions and which are not applicable to the structure in the signals in our problem. Here, instead we impose constraints on the reflectivity profile x and transmitted waveform h to regularize the inversion problem. Specifically, we know that the transmitted pulse his nearly bandlimited such that the energy of the signal in the frequencies outside the passband is sufficiently small. In addition, h is also known to have short time duration, i.e., without loss of generality, all the signal energy is reserved in the first  $T \ll N$  samples of **h**. By explicitly enforcing this structure we can avoid the trivial global minimum discussed earlier. Constraints on the transmitted waveform can be augmented with prior information about the structure of the reflectivity profile x. In the next section, we briefly review EM wave propagation in layered dielectric media and show that sparsity in reflectivity profile x follows directly from the underlying phenomenology.

# A. Multilayer Propagation Model

We consider a one dimensional setting, where an EM wave traveling through the x-axis at spatial position  $x_0$  is represented as a complex exponential,  $E_0 = Ae^{j(kx_0-wt)}$ , where  $A \in \mathbb{R}$  is the amplitude, k (rad/m) denotes the wavenumber, w (rad/sec) and t (sec) represent the angular frequency and the time (temporal position) respectively. In Fig. 1, we illustrate the propagation of the EM wave  $E_0$  in a 3-layer structure. Here, for a given medium i, we represent the dielectric properties, i.e., permittivity, permeability and conductivity by  $\varepsilon_i$ ,  $\mu_i$  and  $\sigma_i$  respectively. If multiple boundaries separating different media exist, then the resulting backscattered signal is given by the infinite summation of multiple reflections. In the case of Fig. 1, where we have 2 boundaries, the total reflected wave is given by  $E_r = E_0\Gamma_r$ , where  $\Gamma_r$  is of the form

$$\Gamma_r = r_{01} + t_{01} t_{10} r_{12} e^{-\gamma_1} e^{-jw\beta_1} \left[ \sum_{k=0}^{\infty} \left( r_{10} r_{12} e^{-\gamma_1} e^{-jw\beta_1} \right)^k \right], \tag{2}$$

where  $t_{ij}=2n_i/(n_i+n_j)$  and  $r_{ij}=(n_i-n_j)/(n_i+n_j)$  represent the transmission and reflection coefficients from medium i to medium j. Here  $\beta_1=2d_1n_1$  is the two-way delay and  $n_1=\sqrt{\varepsilon_1\mu_1}$  is the refractive index of medium 1. The loss index  $\gamma_1$  is approximated as  $\gamma_1\approx d_1\sigma_1\sqrt{\mu_1/\varepsilon_1}$ . For multilayer structures, since the reflected wave energy significantly drops after a certain number of reflections, (2) can be generalized in the following truncated form

$$\Gamma_r = \sum_{k=1}^K \alpha_k e^{-jw\theta_k},\tag{3}$$

where the effects of all propagation losses are combined into the coefficients  $\alpha_k \in \mathbb{R}$  and the arbitrary time delays are given by  $\theta_k \in [0, N-T]$ . This observation reveals that the reflectivity

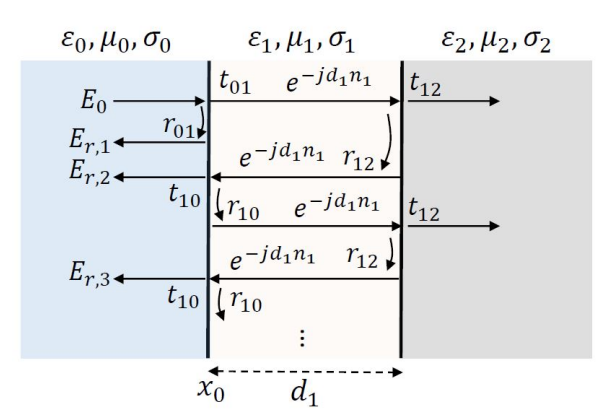


Fig. 1: Multilayer Propagation Model.

profile x consists of impulses in time domain at locations  $\theta_k$ 's with amplitudes  $\alpha_k$ 's. By discretizing the range of  $\theta_k$ 's, we can form a sparse approximation to the summation term in (3)

$$\sum_{k=1}^{K} \alpha_k e^{-jw\theta_k} \approx \mathbf{\Theta}_{\boldsymbol{w}} \boldsymbol{x} \text{ for } w = 0, 1, ..., N - T,$$
 (4)

where  $\Theta_{\boldsymbol{w}} = [1, e^{-jw1}, ..., e^{-jw(N-T)}]^T$  corresponds to first N-T+1 elements of one row of the  $N\times N$  DFT matrix  $\boldsymbol{F}$  and  $\boldsymbol{x}\in\mathbb{R}^{N-T+1}$  represents the K-sparse time domain reflection coefficients. Using the DFT matrix  $\boldsymbol{F}$ , the measurements (1) can be represented in the frequency domain as

$$Fy = \operatorname{diag}(Fh)Fx. \tag{5}$$

Here, h and x are zero-padded accordingly to have proper dimensions in (5). The above discussion reveals the structure of h and x, which can be used to regularize the inversion process. Specifically, h is a short pulse in time domain with a nearly bandlimited frequency spectrum whereas x is a sparse vector. In the next section, we introduce two different approaches exploiting these structures to recover h and x jointly from the measurement y.

# III. JOINT RECOVERY OF TRANSMITTED WAVEFORM AND REFLECTION COEFFICIENTS

This section introduces two different approaches to jointly recover the transmitted pulse and the reflection coefficients. The sensor measurements are modeled in the frequency domain as

$$FY = \operatorname{diag}(Fh)FX, \tag{6}$$

where  $\boldsymbol{Y} \in \mathbb{R}^{N \times L}$  is the time domain measurement matrix, where  $\ell^{th}$  column corresponds to the  $\ell^{th}$  measurement,  $\boldsymbol{h} \in \mathbb{R}^N$  is the time domain transmitted pulse and  $\ell^{th}$  column of matrix  $\boldsymbol{X} \in \mathbb{R}^{N \times L}$  is the impulse response of the reflectivity profile corresponding to the  $\ell^{th}$  measurement. The goal is to recover both  $\boldsymbol{h}$  and  $\boldsymbol{X}$  from the observed measurements  $\boldsymbol{Y}$ . One can easily construct the following optimization problem using (6),

$$\underset{h}{\operatorname{arg\,min}} \| FY - \operatorname{diag}(Fh)FX \|_F^2, \tag{7}$$

where  $\boldsymbol{X} = [\boldsymbol{x}_1, \boldsymbol{x}_2, ..., \boldsymbol{x}_L]$  and  $\boldsymbol{x}_i \in \mathbb{R}^N$ . However, this formulation does not utilize any of our prior knowledge on the optimization variables  $\boldsymbol{X}$  and  $\boldsymbol{h}$ . Moreover, because of its non-convex structure, convergence to global minima is not guaranteed and we cannot use the merits of convex optimization algorithms. To overcome these problems, in the following sections, we provide two different approaches that i) transforms the problem into a convex optimization problem while partially utilizing our prior knowledge and ii) enforces several constraints to fully utilize our prior knowledge in a non-convex setting. Before proceeding to the next sections, we note that any solution to this problem still suffers from the scaling ambiguity, i.e., both  $(\lambda \boldsymbol{h}, \frac{1}{\lambda} \boldsymbol{X})$  and  $(\boldsymbol{h}, \boldsymbol{X})$  yields the same measurements  $\boldsymbol{Y}$  for any scalar  $\lambda$ . Therefore, both approaches presented below recover  $\boldsymbol{h}$  and  $\boldsymbol{X}$  up to a scale.

# A. Approach 1

We first convert the bilinear structure of (7) into a linear form by applying a simple trick [12], [13]. First, we construct the  $M \times N$  dimensional partial DFT matrix  $\mathbf{F}_{\Omega}$  by taking the M rows of  $\mathbf{F}$  corresponding to the passband  $\Omega$ . Assuming  $\mathbf{F}_{\Omega}\mathbf{h}$  is nonzero, define  $\mathrm{diag}(\Delta_h) = \mathrm{diag}(\mathbf{F}_{\Omega}\mathbf{h})^{-1}$ , i.e.,  $\Delta_h \in \mathbb{C}^M$  is the entry-wise inverse of  $\mathbf{F}_{\Omega}\mathbf{h}$ . Replacing  $\mathbf{F}$  by  $\mathbf{F}_{\Omega}$  in (6) and multiplying by  $\mathrm{diag}(\Delta_h)$  from left yields

$$\operatorname{diag}(\Delta_h) \boldsymbol{F}_{\Omega} \boldsymbol{Y} = \boldsymbol{F}_{\Omega} \boldsymbol{X}. \tag{8}$$

By this rearrangement, we achieved a linear equation on both  $\Delta_h$  and X. However, (8) admits the trivial solution of  $\Delta_h = \mathbf{0}_{M\times 1}$  and  $X = \mathbf{0}_{N\times L}$ . In order to eliminate this trivial solution, we can introduce a convex constraint which is of the form  $\mathbf{1}^T\Delta_h = M$ , where  $\mathbf{1} = [1,1,\ldots,1]^T$  with properly selected length. Since we use  $F_\Omega$  instead of F, the bandlimited structure of h is explicitly enforced. Sparsity of X can be exploited by minimizing the  $\ell_0$ -norm. However, since  $\ell_0$ -norm minimization is i) not convex and ii) not feasible in practice, we use the  $\ell_1$ -norm, which is the convex relaxation of  $\ell_0$ -norm. Now, we can construct the following blind recovery problem as in [12]

$$\underset{\Delta_h, \boldsymbol{X}}{\arg\min} \|\operatorname{diag}(\Delta_h)\boldsymbol{F}_{\Omega}\boldsymbol{Y} - \boldsymbol{F}_{\Omega}\boldsymbol{X}\|_F^2 + \lambda \|\boldsymbol{X}\|_1$$

$$\underset{\text{subject to}}{\Delta_h, \boldsymbol{X}} \tag{9}$$

where  $\lambda$  is the regularization parameter. Since this problem is both linear and convex on the optimization parameters, we can use off-the-shelf algorithms to solve for both  $\Delta_h$  and  $\boldsymbol{X}$ . After  $\Delta_h$  is being found, we can easily convert it back to  $\boldsymbol{F}_{\Omega}\boldsymbol{h}$  and take the inverse Fourier transform to obtain the time domain pulse  $\boldsymbol{h}$ .

In this approach, both bandlimited structure of h and the sparsity of X are utilized. We also note that there exists another trivial solution other than  $(\Delta_h, X) = (\mathbf{0}_{M \times 1}, \mathbf{0}_{N \times L})$  when L = 1, i.e., we have only one measurement. This is the case where X is a single impulse and  $\Delta_h$  is the entry wise inverse of  $F_\Omega Y$ . Hence, at least two different measurements, i.e., L = 2, are required in this approach.

# B. Approach 2

As discussed in the previous section, the main problem in solving this bi-convex problem lies in the case of the trivial global optima. In the convex formulation presented above, this global solution was excluded from the constraint set by utilizing multiple measurement vectors. In this non-convex formulation we further encode additional structure in the transmitted waveform namely the shortness in duration of the transmitted pulse in the ultra-wideband setting. This problem of sparse blind deconvolution problem has been recently analyzed in [14], [15] where the short duration of the input pulse is used to avoid the trivial global optima. In order to reduce the effects on scale ambiguity, we further enforce the unit norm constraint on the energy of the transmitted pulse. This sphere constraint leads to a non-convex constraint set but this approach provides a method to enforce the shortness constraint in time-domain for the transmitted pulse. The optimization problem is given as follows

arg min 
$$\|\mathbf{F}\mathbf{Y} - \operatorname{diag}(\mathbf{F}\mathbf{h})\mathbf{F}\mathbf{X}\|_{F}^{2} + \lambda \|\mathbf{X}\|_{1}$$
  
 $\mathbf{h}, \mathbf{X}$  (10)  
subject to  $\|\mathbf{h}\|_{2}^{2} = 1$ ,  $\|\mathbf{h}_{T^{C}}\|_{2}^{2} \leq \epsilon$ ,

where  $\lambda$  is the regularizing constant,  $T^{C}$  is the complement of the support set T in time domain where the transmitted waveform is non-zero and  $\epsilon$  represents the energy of the transmitted signal outside the pulse duration. The bilinear problem in (10) is solved using the block-wise coordinate descent method, which has been analyzed in solving multiconvex problems in [16]. Therefore, the optimization problem is solved by alternating between optimization of the reflection coefficients using the current estimate of the transmitted pulse and subsequently updating the estimate of the transmitted pulse while keeping the reflection coefficients fixed. The optimization problem in estimating the reflection coefficients involves solving an  $\ell_1$  regularized problem. The estimation of the transmitted pulse involves solving the convex optimization problem on the surface of the sphere, therefore a simple projected gradient method is used to solve the problem. The next section presents the performance of the proposed methods to recover the transmitted pulse as well as the reflectivity profile on simulated as well as real data.

# IV. RESULTS

In this section, we illustrate the performance of the presented approaches using experiments with measured and simulated data. In each case, 96% of the transmitted pulse energy is occupied in the band of 0.5-3.5 GHz, i.e., the transmitted pulse is nearly bandlimited, and a sampling rate of 36 GSamples/sec is used to obtain 512 samples of the received backscatter signal. Here, note that we normalized all the recovery results and the ground truths to eliminate the effect of scaling ambiguity in illustrations.

# A. Numerical Experiments

In the first set of experiments, we use randomly generated measurements. We first generate a Gaussian pulse and obtain

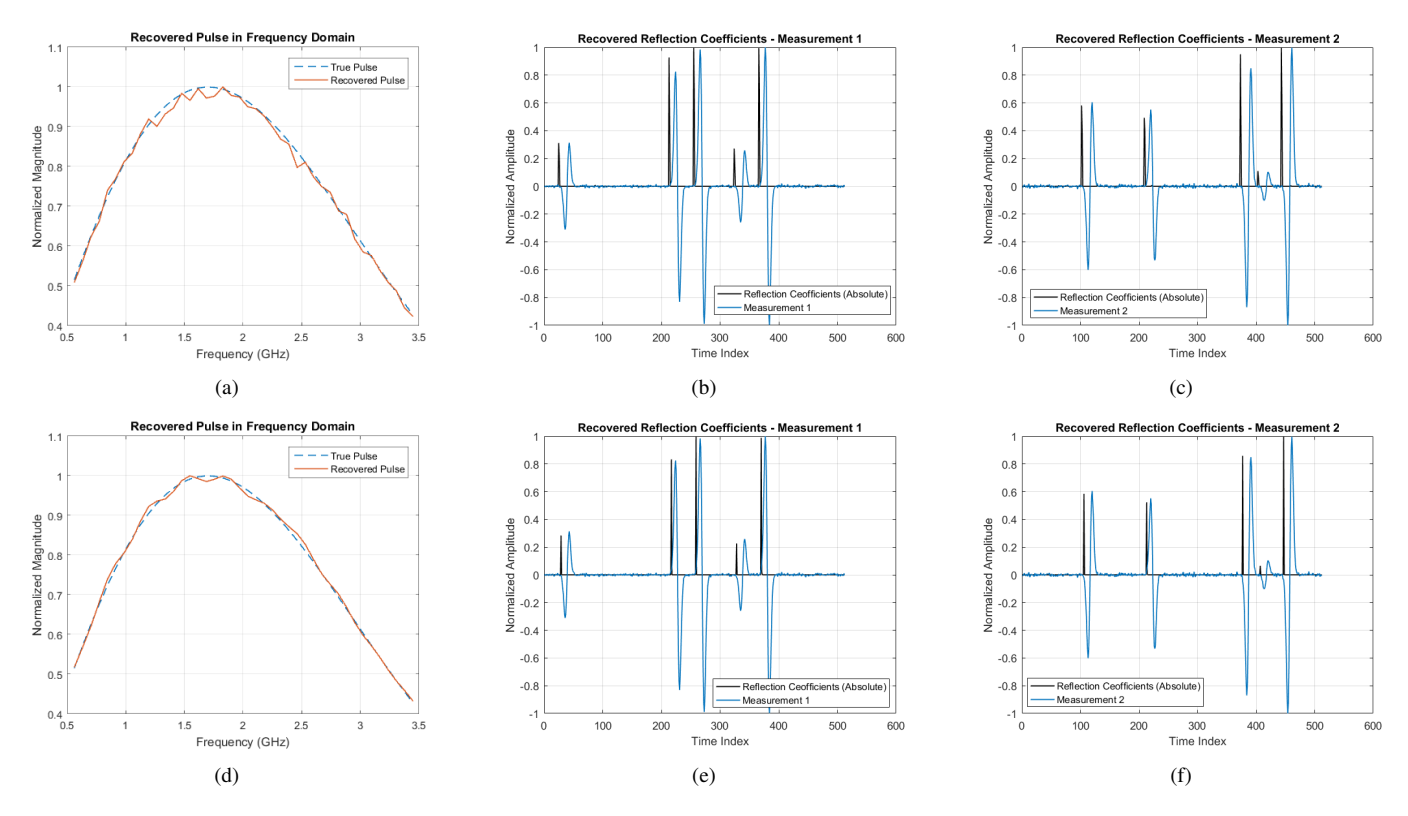


Fig. 2: Recovery results for randomly generated measurements. (a),(d): Pulse recovery in frequency domain using Approach 1 and 2 respectively. (b),(c): Recovered reflection coefficients using Approach 1 for L = 2 case. (e),(f): Recovered reflection coefficients using Approach 2 for L = 2 case.

the measurements by convolving this pulse with a random set of reflection coefficients. Both the amplitudes and the positions of the reflection coefficients are randomly generated using the uniform distributions U[-1,1] and U[0,N-T+1] respectively. For all measurements, the number of spikes is fixed to be 5. We also add white Gaussian noise to all the measurements such that the signal-to-noise ratio (SNR) is fixed to 30dB. We illustrate the random measurements and the corresponding recovery results in Fig. 2. We observe that both the convex and the non-convex approaches recover the original transmitted waveform accurately in the frequency domain. We also observe that the positions and the magnitudes of the reflection coefficients are successfully recovered.

In the second part of the experiments, we use measurements that simulates the real-life reflections from layered human tissues. We have worked on three different cases, *i)* single layer of skin tissue, *ii)* two layers of skin and bone tissues, *iii)* three layers of skin, bone and muscle tissues. For all cases, we assume that there is an infinite length medium with known permittivity, which we call absorber, at the inner-most layer and all the tissues have a thickness of 1 cm. In Fig. 4, both ground truth reflectivity profile and the recovery results for the reflection coefficients are represented. Note that we observe multiple reflections even for the single skin tissue case, which is caused by the skin-absorber interface.

In the third part, we work with measurements collected from

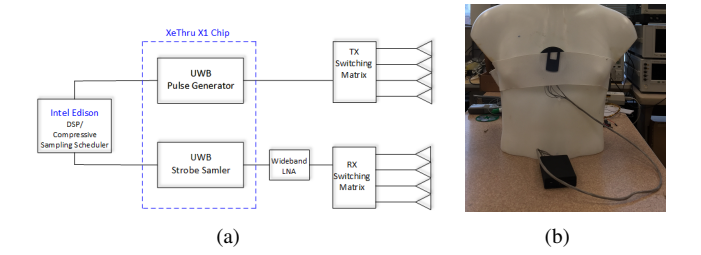


Fig. 3: (a): The block diagram of the system used to generate ultra-wideband signal. (b): The designed system, which is used to analyze the structure and dielectric properties of the Thoracic cavity.

a test subject using the radar sensor *Easysense*. This sensor is used to obtain backscattered measurements of the thoracic cavity. These measurements are used to analyze the tissue layer structure and study the dielectric properties of lungs. This provides a non-invasive method to study the tissue layers.

# B. Measured Data Experiments

Measurements are obtained using an experimental ultrawideband micro-radar platform dubbed as EasySense. Easy-Sense utilizes an UWB pulse generator and a strobe sampler. It includes two 1x4 antenna switching matrices that connects to two sets of four wideband antennas. The receive frontend includes wideband Low Noise Amplifier (LNA) making it

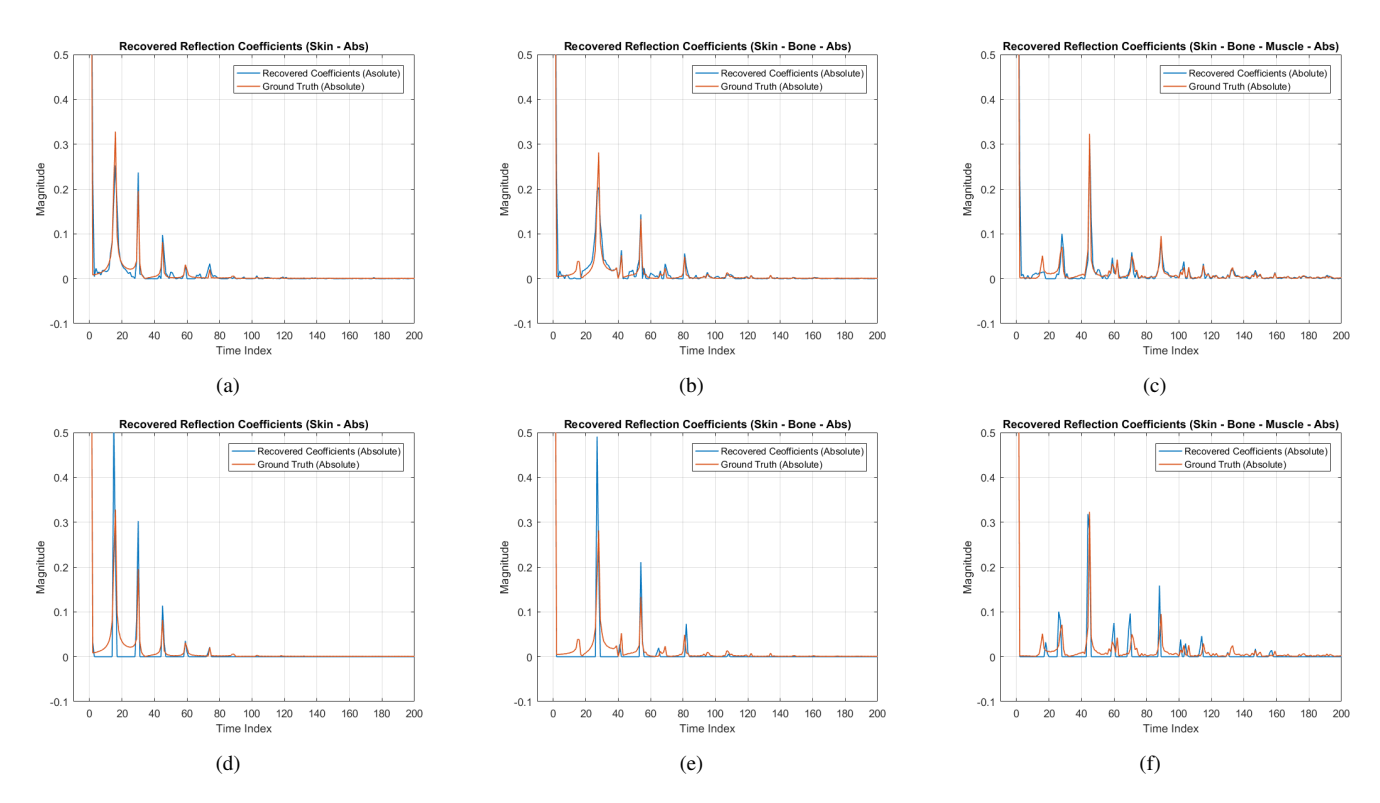


Fig. 4: Recovered reflection coefficients for simulated measurements. (a),(b),(c): Recovery results for Skin, Skin-Bone, Skin-Bone-Muscle cases respectively using Approach 1. (d),(e),(f): Recovery results for Skin, Skin-Bone, Skin-Bone-Muscle cases respectively using Approach 2.

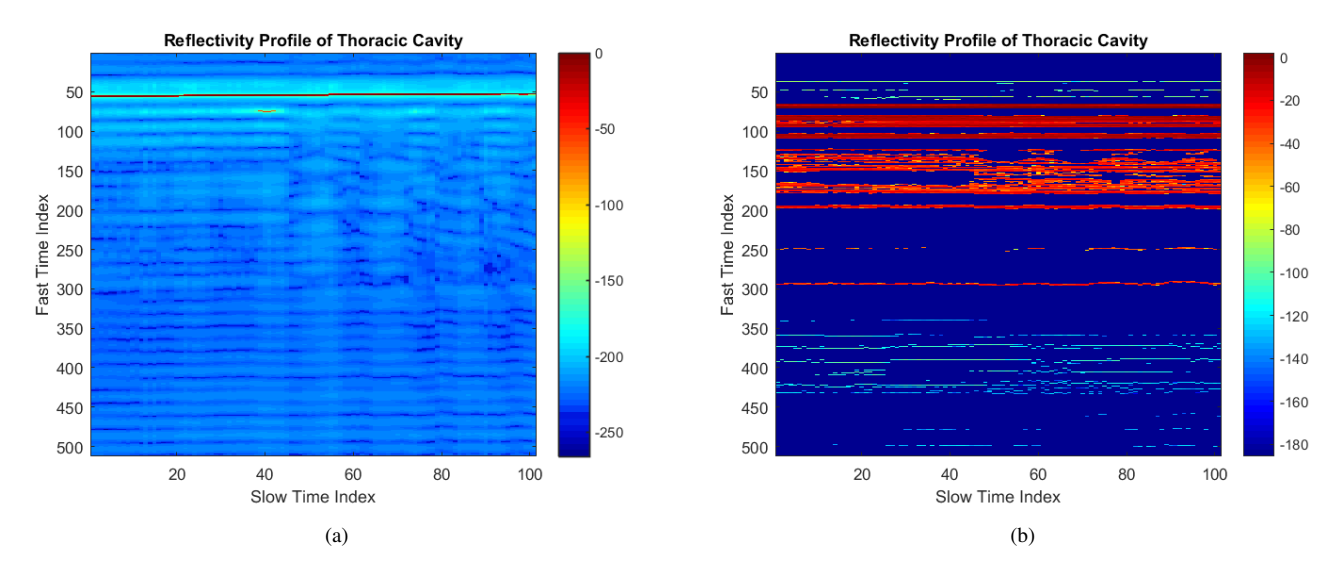
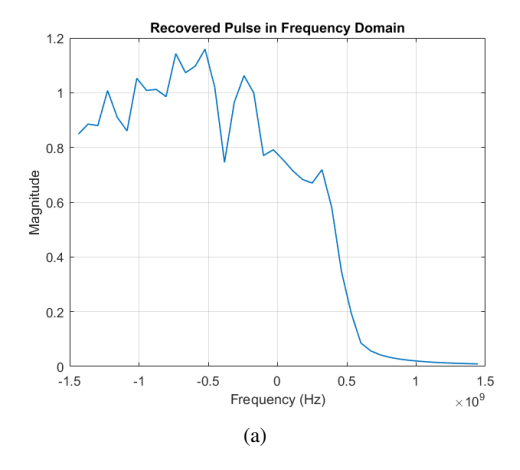


Fig. 5: Recovery results for the reflection coefficients from the thoracic cavity using Approach 1 (a) and Approach 2 (b).

suitable for field measurements. The UWB pulse generator produces monocycle pulses and samples the returns on a window of 512 samples using strobe-sampling at a virtual rate of 36 Gsamples/sec. The block diagram of the Easy-Sense hardware is given in Fig. 3(a) and an image of the measurement setup is shown in Fig. 3(b). The measurements are obtained by using the EasySense radar sensor to monitor the thoracic cavity of a test subject. The subject is asked to

hold his breath during the first half of the measurement period while being asked to breath regularly for the second half. The pulse repetition frequency (PRF) used in this setup is 100 Hz. This PRF is sufficient to capture the low frequency respiration signal due to the movement of the tissue layers. Since the backscattered signal is a superposition of the transmitted signal from multiple bounces within these layers, we expect to see the respiration signal across the measurements to repeat after



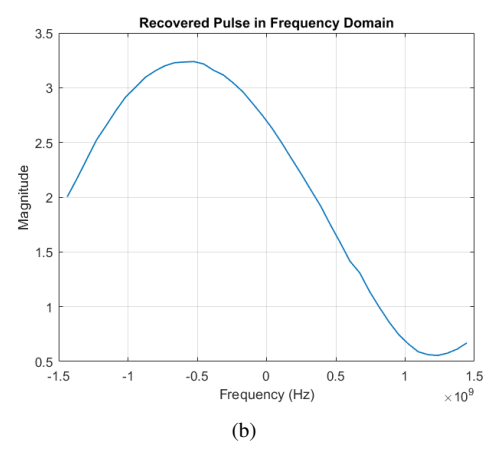


Fig. 6: Recovery results for the transmitted waveform from the thoracic cavity measurements using Approach 1 (a) and Approach 2 (b).

a certain depth in the tissue layers. Since the transfer function of the antenna interface with the skin tissue is unknown, we jointly estimate the resultant transmitted signal convolved with this unknown transfer function of the antenna-skin interface as well as the transfer function representing the tissue layers. We illustrate the recovered reflectivity profiles of thoracic cavity in Fig. 5. We observe that both approaches accurately identify the breathing and the non-breathing cycles. We also observe that the respiration pattern repeats in deeper layers due to the multiple bounces. In Fig. 6, we have the complex baseband representation of the recovery results for the transmitted waveform in frequency domain. We observe that both approaches recover a bandlimited waveform.

# V. CONCLUSION

In this paper we formulated the problem of jointly recovering the transmitted pulse along with the impulse response representing the tissue profile. We derived convex and nonconvex formulations for this bilinear problem and introduced constraints to avoid ambiguities and trivial solutions. We evaluated the performance of the proposed approaches using expereiments with simulated and measured data. For future research, we aim to establish theoretical guarantees for the

proposed convex formulations and study the sample complexity in terms of the number of snapshots and measurements to successfully recover the unknown signals. Furthermore, we aim to extend the lifting framework proposed in [17] to encode the structure present in our problem. Finally, we are interested in analyzing the non-convex formulation of the sparse blind deconvolution problem and study the geometry and establish properties of the local optima following recent work presented in [15].

#### ACKNOWLEDGMENT

This research was in part supported by grant U54EB020404 awarded by the National Institute of Biomedical Imaging and Bioengineering.

#### REFERENCES

- [1] A. Mokdad, J. Marks, D. Stroup, and J. Gerberding, "Actual causes of death in the united states, 2000," JAMA: the journal of the American Medical Association, vol. 291, no. 10, p. 1238, 2004.
- [2] J. Gao, S. Baskar, D. Teng, M. alAbsi, S. Kumar, and E. Ertin, "A new direction for biosensing: Rf sensors for monitoring cardio-pulmonary function," in *Mobile Health*. Springer, 2017, pp. 289–312.
- [3] J. Gao, E. Ertin, S. Kumar, and M. al'Absi, "Contactless sensing of physiological signals using wideband rf probes," in 2013 Asilomar Conference on Signals, Systems and Computers. IEEE, 2013, pp. 86– 90
- [4] E. M. Staderini, "UWB radars in medicine," *IEEE Aerospace and Electronic Systems Magazine*, vol. 17, no. 1, pp. 13–18, 2002.
- [5] S. A. T. Hosseini and H. Amindavar, "Uwb radar signal processing in measurement of heartbeat features," in *IEEE International Conference* on Acoustics, Speech and Signal Processing, 2017, pp. 1004–1007.
- [6] S. Choudhary and U. Mitra, "On the properties of the rank-two null space of nonsparse and canonical-sparse blind deconvolution," *IEEE Transactions on Signal Processing*, vol. 66, no. 14, pp. 3696–3709, July 2018.
- [7] —, "Fundamental limits of blind deconvolution part I: ambiguity kernel," CoRR, vol. abs/1411.3810, 2014.
- [8] —, "Fundamental limits of blind deconvolution part II: sparsity-ambiguity trade-offs," CoRR, vol. abs/1503.03184, 2015.
- [9] A. Benichoux, E. Vincent, and R. Gribonval, "A fundamental pitfall in blind deconvolution with sparse and shift-invariant priors," in 2013 IEEE International Conference on Acoustics, Speech and Signal Processing, May 2013
- [10] Y. Li, K. Lee, and Y. Bresler, "Identifiability in blind deconvolution with subspace or sparsity constraints," *IEEE Transactions on Information Theory*, vol. 62, no. 7, pp. 4266–4275, July 2016.
- [11] ——, "Identifiability and stability in blind deconvolution under minimal assumptions," *IEEE Transactions on Information Theory*, vol. 63, no. 7, pp. 4619–4633, July 2017.
- [12] R. Gribonval, G. Chardon, and L. Daudet, "Blind calibration for compressed sensing by convex optimization," in 2012 IEEE International Conference on Acoustics, Speech and Signal Processing (ICASSP), March 2012, pp. 2713–2716.
- [13] L. Wang and Y. Chi, "Blind deconvolution from multiple sparse inputs," IEEE Signal Processing Letters, vol. 23, no. 10, pp. 1384–1388, Oct 2016.
- [14] H. Kuo, Y. Lau, Y. Zhang, and J. Wright, "Geometry and symmetry in short-and-sparse deconvolution," preprint, https://arxiv.org/abs/1901.00256, 2019.
- [15] Y. Zhang, Y. Lau, H. Kuo, S. Cheung, A. Pasupathy, and J. Wright, "On the global geometry of sphere-constrained sparse blind deconvolution," in 2017 IEEE Conference on Computer Vision and Pattern Recognition (CVPR), July 2017, pp. 4381–4389.
- [16] Y. Xu and W. Yin, "A block coordinate descent method for regularized multiconvex optimization with applications to nonnegative tensor factorization and completion," SIAM J. Imaging Sciences, vol. 6, pp. 1758–1789, 2013.
- [17] A. Ahmed, B. Recht, and J. Romberg, "Blind deconvolution using convex programming," *IEEE Transactions on Information Theory*, vol. 60, no. 3, pp. 1711–1732, March 2014.